HHS Public Access

Author manuscript

Adv Mater. Author manuscript; available in PMC 2021 October 01.

Published in final edited form as:

Adv Mater. 2020 October ; 32(43): e2001628. doi:10.1002/adma.202001628.

An adhesive hydrogel with "load-sharing" effect as tissue bandages for drug and cell delivery

Jing Chen,
Department of Biological and Environmental Engineering, Cornell University, Ithaca, NY 14853, USA

Dong Wang,
Department of Biological and Environmental Engineering, Cornell University, Ithaca, NY 14853, USA

Long-Hai Wang,
Department of Biological and Environmental Engineering, Cornell University, Ithaca, NY 14853, USA

Wanjun Liu,
Department of Biological and Environmental Engineering, Cornell University, Ithaca, NY 14853, USA

Alan Chiu,
Department of Biological and Environmental Engineering, Cornell University, Ithaca, NY 14853, USA

Kaavian Shariati,
Department of Biological and Environmental Engineering, Cornell University, Ithaca, NY 14853, USA

Qingsheng Liu,
Department of Biological and Environmental Engineering, Cornell University, Ithaca, NY 14853, USA

Xi Wang,
Department of Biological and Environmental Engineering, Cornell University, Ithaca, NY 14853, USA

Zhe Zhong,
Department of Biological and Environmental Engineering, Cornell University, Ithaca, NY 14853, USA

James Webb,
Department of Biological and Environmental Engineering, Cornell University, Ithaca, NY 14853, USA

[*] Corresponding authors. : mm826@cornell.edu (M. Ma).

Supporting Information

Supporting Information is available from the Wiley Online Library or from the author.

Robert E. Schwartz,
Division of Gastroenterology and Hepatology, Weill Cornell Medical College, New York, NY 10065, USA

Nikolaos Bouklas,
The Sibley School of Mechanical and Aerospace Engineering, Cornell University, Ithaca, NY 14853, USA

Minglin Ma*
Department of Biological and Environmental Engineering, Cornell University, Ithaca, NY 14853, USA

Abstract

Hydrogels with adhesive properties have potentials for numerous biomedical applications. Here we report the design of a novel, intrinsically adhesive hydrogel and its use in developing internal therapeutic bandages. The design involves incorporation of “triple hydrogen bonding clusters” (THBC) as side groups into the hydrogel matrix. The THBC through a unique “load sharing” effect and an increase in bond density resulted in strong adhesions of the hydrogel to a range of surfaces including glass, plastic, wood, PTFE, stainless steel and biological tissues even without any chemical reaction. Using the adhesive hydrogel, we developed tissue adhesive bandages for either targeted and sustained release of chemotherapeutic nano-drug for liver cancer treatment or anchored delivery of pancreatic islets for a potential type 1 diabetes (T1D) cell replacement therapy. Stable adhesion of the bandage inside the body enabled almost complete tumor suppression in an orthotopic liver cancer mouse model and ~1-month diabetes correction in chemically induced diabetic mice.

Graphical Abstract

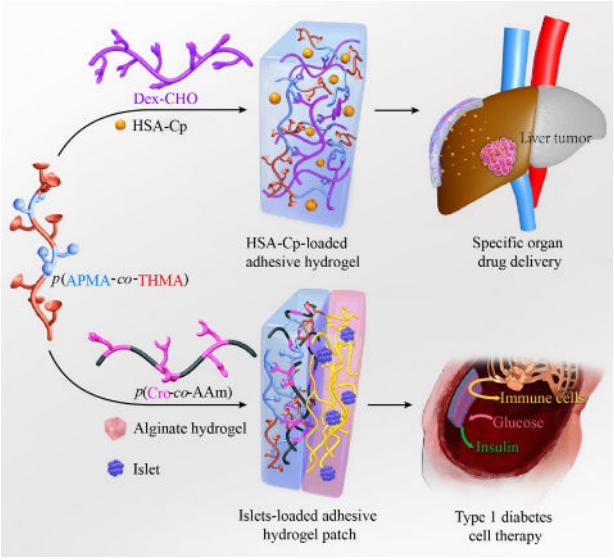

Internally applied tissue bandages based on a novel adhesive hydrogel were developed for delivery of either anti-tumor drugs directly to the tumor site or insulin-producing cells to treat type 1 diabetes.

Keywords

load sharing; tissue bandages; adhesive hydrogels; targeted delivery; type 1 diabetes

Hydrogels with high water content and biocompatibility have various applications in fields of biomedicine such as cancer[1], diabetes[2], and cardiovascular disease[3]. Incorporating adhesive properties into hydrogels can either augment or expand the applications significantly[4]. For example, Li developed a family of tough adhesive hydrogels by forming amide bond for various applications including tissue adhesives, wound dressing, and tissue repair[5]. Based on a similar chemistry, dry double-sided hydrogel tape was made from a combination of a biopolymer (gelatin or chitosan) and crosslinked poly(acrylic acid) grafted with N-hydrosuccinimide ester[6], which exhibited strong adhesions on engineered solids or wet tissues within five seconds of application. While all the previous work clearly demonstrated the tremendous potential of adhesive hydrogels, the adhesion was mostly based on direct chemical reactions between the hydrogel and the substrate, with energy dissipation in the bulk. Adhesive hydrogels based on physical interactions were also developed such as those involving mussel-inspired catechol functional groups[7]. For example, paintable hydrogel constructed through Fe^{3+}-triggered simultaneous polymerization of covalently linked pyrrole and dopamine was developed for sealing the heart without adverse liquid leakage[8]. However, catechol groups are easy to be oxidized to quinone groups by oxygen in the air, which may limit their long-term and repeatable adhesion property. In order to address this problem, silver-pectin nanoparticles were incorporated into the hydrogels to control the redox balance of the catechol groups. These hydrogels showed high antibacterial activity for effective wood healing applications despite potential concerns on the toxicity of silver ions[9].

Here we report a new adhesive hydrogel with high H-bond density that takes advantage of a load sharing effect of “triple hydrogen bonding clusters” (THBC). When incorporated as side groups into the hydrogel matrix, the THBC resulted in strong adhesions of the hydrogel to a range of surfaces including glasses and tissues even without any chemical reaction. Importantly, based on this type of hydrogel, we developed two innovative, therapeutic, bandage-like medical devices for treatment of liver cancer and type 1 diabetes, respectively. We demonstrated in an orthotopic liver cancer model, a biodegradable hydrogel bandage encapsulating a human serum albumin (HSA) conjugated cisplatin nano-drug (HCp) adhered to the liver before degradation and provided sustained delivery directly to the tumor site, leading to significantly improved therapeutic outcome than systemic injection. On the other hand, a non-degradable bandage with an adhesive hydrogel layer and an islet encapsulating layer was shown to adhere to the peritoneal body wall for at least 1 month and provided robust control of blood glucose level in a diabetic mouse model. These internal hydrogel bandages represent a versatile platform for targeted and sustained drug delivery for treatment and post-surgical care of solid tumors as well as anchored delivery of pancreatic islets for a potential type 1 diabetes (T1D) cell replacement therapy.

The key component to our adhesive hydrogel is the N-[Tris(hydroxymethyl)methyl]acrylamide (THMA) which contains three hydroxy groups

clustered together. We co-polymerized THMA with N-(3-Aminopropyl)methacrylamide hydrochloride (APMA) which was chosen to facilitate crosslinking and salt displacement (Figure S1)[10]. The copolymerization was confirmed by ^{1}H-NMR spectrum (Figure S2). The APMA ratio determined by 2,4,6-trinitrobenzenesulfonic acid (TNBS) method was 18.2% for 80% THMA feed ratio. 30.5% and 45.2% of APMA ratios were determined with same method for 65% and 50% THMA feed ratios, respectively. To obtain a hydrogel which was confirmed by a rheology test (Figure S3), we used a sodium tripolyphosphate (STTP) to ionically crosslink the copolymer (Figure 1A). The THBC adhesive hydrogel adhered to a variety of surfaces, such as glass, plastic, PTFE, stainless steel, wood and rubber (Figure 1B). Moreover, the *p*(APMA-*co*-THMA) hydrogel with 80% THMA was also highly adhesive to mouse liver (Figure 1C), in contrast to other hydrogels involving hydrogen bonding (e.g. *p*APMA, PEI, Chitosan, PAA, *p*THMA and PVA) which all exhibited much lower adhesion to liver (Figure S4). It is of importance to note that the adhesive property of the new hydrogel was achieved without any chemical reactions with the substrate or tissue.

We attribute the adhesive properties of the THBC hydrogel to the high density of hydrogen bonds as well as the unique equal load sharing (ELS) configuration of the THBC (we postulate that each bond in a cluster carries the same force, while forces can vary between the clusters), both of which contribute to increasing the interfacial toughness. In general, the effectiveness of an adhesive is characterized by the interfacial toughness, which dictates the energy to decohere the interface from the substrate by a unit area. For the THBC hydrogel, hydrogen bonds form on the interface but they are also present in the bulk of the adhesive layer (Figure 1D). Having hydrogen bonds in the bulk, which are able to break and reform during loading provides an additional energy dissipation mechanism, on top of bond breaking exactly at the interface. The total interfacial toughness can be expressed as $\Gamma = \Gamma_0 + \Gamma_D$, where Γ_0 is the intrinsic interfacial toughness attributed to rupture of bonds directly attaching the hydrogel adhesive to the substrate and Γ_D the dissipation due to rupture of bonds of the adhesive in the bulk. This interpretation builds on the work by Zhang et[11] where they considered Γ_D is due to bulk dissipation in one of the adhered layers during loading, but in our work we consider the adhesive layer itself as a network that has the potential to dissipate energy both on the interfaces and in the bulk through the rupture of hydrogen bonds. The potential of the hydrogen bonds to break and reform will also contribute to the enhancement of Γ_D. Increasing the density of H-bonds per monomer (considering that monomers occupy the same volume) will directly enhance both Γ_0 and Γ_D [12]. More importantly, Γ_0 is enhanced due to the unique ELS configuration of THBC compared to a homogeneous distribution of H-bonds given the same total bond density. We show through an atomistically informed continuum model for fracture by Möller and Bitzek[13] that the interface with THBC or load sharing is tougher than that with a homogeneous spatial distribution of bonds even though the macroscopic density of the bonds is equal (Figure 1E, 1F) (see Supporting Information for details).

Next, we sought applications of the THBC hydrogel for tissue bandages. However, it was found that the STTP-crosslinking due to the ionic nature lacked the necessary stability under physiological conditions (e.g. in saline), which made it challenging for long-term *in vivo*

applications. Therefore, we used an oxidized dextran (Dex-CHO) to chemically crosslink the same *p*(APMA-*co*-THMA) copolymer to enhance its stability (Figure 2A). Dex-CHO was synthesized through oxidizing the hydroxyl groups in the presence of sodium periodate (Figures S5, S6). The hydrogel strongly adhered to two glass slides indicating that its adhesive property remained after Dex-CHO crosslinking (Figure 2B). The maximum adhesion energy, measured using a peeling test (Figure 2C), increased with the content of THMA (Figure 2D), and a maximum adhesion energy of 422 Jm^{-2} was achieved for the hydrogel with 80% THMA, larger than that of 65% or 50% THMA (289 and 145 Jm^{-2}, respectively). The adhesion strength, evaluated by a lap-shear test (Figure 2E), increased with the ratio of NH_2/CHO, with the maximum reaching 85.1 KPa at the NH_2/CHO ratio of 1.2 (Figure 2F), about 40-fold higher than a previously published adhesive hydrogel with NH_2/CHO crosslinking [14]. When fixing the NH_2/CHO ratio at 1.2 and varying the solid content in the hydrogel from 5 to 30%, we found that the hydrogel had the highest adhesion strength (~118 KPa) at an optimal solid content of 20%. (Figure 2G). At a lower solid content, the hydrogel might have weaker bulk strength and lower cohesion failure strength, while above 20%, excessive physical crosslinking could limit the mobility of the polymer chains, thereby resulting in decreased contacts of the hydrogel to the substrate and the adhesion strength. The hydrogel reached an equilibrium swollen state after ~72 hours of immersion in PBS at 37 °C with a swelling ratio of 1.47 (Figure S7). We also examined the influence of storage time in saline on the adhesion strength in order to mimic the body fluid condition. The hydrogels were prepared, sealed in a flask containing saline and placed under 37 °C for 7, 14, and 30 d (Figure 2H). Lap-shear results showed that the hydrogels after storing for different amounts of time maintained almost the same adhesion strengths to glass slides as the freshly prepared gels, suggesting that the hydrogel might overcome the disadvantage of catechol-based adhesive hydrogels that tended to gradually lose adhesion ability due to oxidation of catechol groups. Lastly, we confirmed the hydrogel was highly adhesive to biological tissues including kidney, spleen and liver (Figure 2I). Even under 30 second running water directed at the top of the hydrogel, it remained adhered to the liver tissue (Figure 2J, Video V1). Although the tissue adhesion observed here might be partially due to the reaction between any unreacted CHO groups in the hydrogel with the tissue surface amines, the ELS effect of the THBC and the high H-bond density likely played an important role similar to the case of STTP-crosslinked hydrogels where there was no chemical reaction between the hydrogel and tissue. Additional mechanical tests of the THBC hydrogel including tensile stress, fracture energy and compressive stress confirmed the resilience of the hydrogel (Figure S8-S10), which may also contribute to the strong interfacial adhesion.

To take advantage of tissue adhesive property and demonstrate the therapeutic potential of our hydrogel, we designed an internal bandage with organ-specific, sustained drug release and chose in a first application liver cancer as our model. Liver cancer is a leading malignancy globally and has a poor five-year survival rate of less than 20%[15]. Currently, the most common liver cancers are hepatocellular carcinoma (HCC). Surgical ablation is the most commonly used treatment for HCC[16]. However, small tumor nodules could remain after surgical resection, grow and cause distant metastasis[17]. Furthermore, the systemic chemotherapeutics generally have a low treatment efficacy for HCC mainly due to fast

clearance and low tumor uptake[18]. Given these challenges, we hypothesized that our *p*(APMA-*co*-THMA)/Dex-CHO adhesive hydrogel bandage could allow drugs to be released directly to the liver, mitigate the fast clearance and improve the tumor uptake (Figure 3A).

Live imaging using IVIS (in vivo imaging system) of internally adhered, Cy5.5-labelled blank hydrogel bandage confirmed the gradual biodegradation within 15 days in mice (Figure. 3B), indicating that the hydrogel bandage could be served as sustained drug delivery depot. Moreover, MTT assays revealed that blank hydrogel bandage was nontoxic toward L929 cells even at a solid content of 30% (Figure S11). To load the anti-tumor drug Cisplatin (Cp) into the hydrogel, we first formulated the drug into nanoparticles by conjugating it to human serum albumin (HCp) according to a previously published method[19]. HSA is the most abundant plasma protein (35–50gL^{-1} human serum) and can target 60 kDa glycoprotein (gp60) receptor and SPARC (secreted protein acid and rich in cysteine)[20]. HCp formed spherical nanoparticle and the average size was around 164 nm with a narrow PDI of 0.128 (Figure 3C). The *in vitro* release studies showed that >70% of cisplatin was released in 24h under the 10 mM Glutathione (GSH) condition (Figure 3D) but with minimal release (~3% in 48 h) under a physiological condition (pH 7.4 and 37 °C) without GSH, indicating that cisplatin release could be triggered in the reductive cytoplasmic environment. Moreover, HCp had a slightly higher IC_{50} (7.97 μM) than free cisplatin (IC_{50}= 4.25 μM) against HepG2 cells, suggesting that HCp could effectively be internalized by the cells with high cytotoxicity (Figure 3E). Fluorescent imaging (Figure 3F) showed Cy5.5-labelled HCp nanoparticles evenly distributed in FITC-labelled adhesive hydrogel bandage.

Subsequently, an orthotopic luciferase-expressing HepG2 (Luc-HepG2) liver cancer model using SCID mice was established to evaluate biodistribution. Cy5.5 and Cy5.5 labelled HCp (or Cy5.5-HCp) were intravenously injected into tumor-bearing mice, while the hydrogel incorporating Cy5.5-HCp (or Cy5.5-HCp-bandage) was adhered directly on the surface of liver. The IVIS fluorescent imaging, 3 days after dosing (Figure 3G), revealed that Cy5.5-HCp-bandage had the brightest signal indicating highest retention of HCp local to the liver tissue. Meanwhile, quantification of the signals in explanted tissues (Figure 3H) confirmed the highest drug retention in the tumor for the Cy5.5-HCp-bandage group. Interestingly, despite high tumor accumulation, relatively low fluorescence was detected in lungs and kidneys. We further histologically analyzed the liver/tumor tissues from the three groups (Figure 3I). Intra-tumor fluorescent signals for the Cy5.5-HCp-bandage group were 5 and 59 times higher than that of Cy5.5-HCp and Cy5.5 groups, respectively (Figure 3J). These results showed that the adhesive hydrogel facilitated sustained drug delivery directly to the tumor site and significantly improved the pharmacokinetics.

In order to evaluate whether the adhesive hydrogel bandage can inhibit tumor growth and improve survival, we performed longer-term experiments, treating orthotopic Luc-HepG2 liver tumor-bearing SCID mice. Cisplatin (3 mg Pt/kg) and HCp (3 mg Pt/kg) were intravenously injected every 3 days for 3 times (on day 0, 3, 6) into the tumor-bearing mice, and HCp-bandage with the same total drug dosage (9 mg Pt/kg) was adhered on the surface of liver. PBS and HSA-loaded adhesive hydrogel bandage (bandage+HSA) were also

included as negative controls. While tumor growth was somewhat inhibited by all cisplatin, HCp and HCp-bandage (Figure 4A, S12), the mice treated with HCp-bandage showed largest inhibition and nearly complete tumor suppression in 21 days. Quantification (Figure 4B) revealed that the HCp-bandage caused a ~6-fold reduction of tumor luminescence as compared to cisplatin or HCp, and a ~13-fold reduction compared to PBS or bandage+HSA. Importantly, in contrast to PBS, bandage+HSA, HCp and cisplatin which led to gradual body weight loss, HCp-bandage caused little change in body weight (Figure 4C). The histological analysis of explanted tissues indicated that the group of HCp-bandage had smaller areas of tumor in the liver and significantly decreased metastasis lesion in the kidney (Figure 4D). Unlike the cisplatin and HCp which caused large areas of necrotic vacuole in the kidney, HCp-bandage had no obvious negative impact to the well-organized kidney tissue confirming its lower side effect; neither did HCp-bandages have any toxicity to the other normal organs including heart, spleen and lung (Figure S13). The staining data was thus consistent with the largely improved median survival time for the HCp-bandage group (54 days), compared to 31 and 36 days for cisplatin and HCp groups, respectively (Figure 4E). All these data together suggest that delivery of cisplatin in a sustained manner directly to the tumor site using our hydrogel bandage could lead to a higher treatment efficacy with less adverse effects.

To demonstrate the versatility of the internal hydrogel bandages, we explored a different therapeutic application – for delivery of insulin-producing cells for type 1 diabetes (T1D) treatment. T1D affects millions of patients and current standard treatments (insulin injection or infusion) are tedious, painful, do not cure the disease or prevent many diabetic complications[21]. Delivery of glucose-responsive, insulin-producing cells using hydrogel microparticles has been considered as a curative therapy, promising to provide long-term and more physiological glycemic control[22]. Unfortunately, hydrogel particles when implanted, usually in the peritoneal cavity, tend to settle and clump due to gravity, causing fibrotic overgrowth and diminishing the mass transfer that is essential for cell function [23]. Thin hydrogel sheets or small diameter hydrogel fibers could provide facile mass transfer, but they may fold, crumple or break in the *in vivo* environment. To address these problems, we developed a “cellular bandage” where a thin alginate hydrogel sheet encapsulating pancreatic islets was glued using the *p*(APMA-*co*-THMA) adhesive hydrogel to the body wall inside the peritoneal cavity.

The cellular bandage had two layers: an adhesive *p*(APMA-*co*-THMA) hydrogel layer crosslinked by a non-biodegradable *p*(Cro-*co*-AAm) and a non-adhesive alginate hydrogel layer where islets would be encapsulated (Figure 5A). *p*(Cro-*co*-AAm) was synthesized by co-polymerizing crotonaldehyde (Cro) and acrylamide (AAm) (Figures S14, S15). A 3D printing mold was made to prepare the bandage (Figure S16). To ensure the two layers bonded together, 50 mM of $CaSO_4$ slurry was loaded inside the adhesive hydrogel layer that slowly released Ca^{2+} to crosslink alginate to form a flat hydrogel sheet (~1.5 mm thick; Figures 5B). 5 mM of $BaCl_2$ was added to adjust the crosslinking speed and enhance the hydrogel stability. Before testing islet encapsulation, we first investigated the adhesive property of cell-free bandages *in vitro* and *in vivo*. The maximum adhesion energy, measured using a peeling test (Figure S17), was about 472 J/m^2, slightly larger than that of bandages without alginate hydrogel coating (452 J/m^2). Afterwards, a cell-free bandage was

implanted on the peritoneal body wall opposing the liver surface (Figure S18). The results showed that the hydrogel bandage adhered to the peritoneal body wall without damage after 10 and 30 days (Figure 5C, S19). In contrast, freely implanted alginate sheets without any anchoring broke and were wrapped by surrounding tissues after one month (Figure S20). Examinations of retrieved samples at 10 days revealed that the adhesive hydrogel layer caused no obvious tissue reaction and there was minimal cellular overgrowth on the alginate surface. Even after 30 days, the fibrotic tissue was relatively thin and no obvious toxicity was observed to normal organs including heart, liver, spleen, lung and kidney (Figure S21).

Using this bi-layer hydrogel bandage, we delivered rat islets into chemically-induced diabetic C57BL/6 mice. Islets with high viability were visible in the alginate layer (Figures 5D, S22). Shortly after transplantation, the blood glucose (BG) level of all the diabetic mice decreased to the normal glycemic range (BG < 200 mg/dL) (Figure. 5E). However, all the mice in the blank hydrogel control group still remained diabetic. While two of the 8 mice experienced earlier failure, six others maintained normoglycemic for 1 month when the implants were retrieved. An intraperitoneal glucose tolerance test (IPGTT) (Figure. 5F), conducted on day 20 after transplantation, demonstrated that the mice with islet bandages cleared blood glucose and restored normoglycemia at a rate comparable to that of non-diabetic mice within 120 min, whereas the BG of diabetic mice failed to drop to normal range even after 180 min. At retrieval, the islet bandages were still adhered to the body wall (Figure. S23). The glucose-stimulated insulin secretion (GSIS) assay performed on the retrieved samples (Figure. 5G) showed that encapsulated islets were functional, secreting insulin in response to glucose stimulation. Histological analysis and immunohistochemistry confirmed the normal morphology of islets with positive staining of insulin and glucagon (Figure 5H).

Several groups have reported adhesive hydrogels based on hydrogen bonding. For example, organic–inorganic hybrid hydrogel polymerized by N-acryloyl 2-glycine and further enhanced by hydroxyapatite showed high adhesion to various substrates. However, the durability *in vivo* was relatively short (less than 14 h)[24]. Moreover, bioinspired adhesive hydrogels tackified by independent nucleobase (adenine, thymine, guanine, cytosine, and uracil) from DNA and RNA were developed in order to circumvent the drawback of dopamine-based adhesion, but long-term adhesion ability and *in vivo* stability are yet to be investigated[25]. There are a few unique features in the hydrogels we present here that are worth reiterating. First, the mechanism for adhesion was attributed to both the high density of hydrogen bonds and the unique ELS configuration of the THBC. In our hydrogels, hydrogen bonds could form on the interface and in the bulk, dissipating energy in both places. Importantly, the ELS effect of the adhesive layer results in tougher adhesion compared to a situation where the same density of bonds are present, but are homogeneously distributed on the interface. Second, we demonstrated three types of adhesive hydrogels all based on the same copolymer *p*(APMA-*co*-THMA): a STTP-crosslinked ionic hydrogel, a biodegradable Dex-CHO-crosslinked one, and a non-degradable *p*(Cro-*co*-AAm)-crosslinked one. Interestingly, they were all adhesive to tissues, even without any chemical reactions in the case of STTP-crosslinked hydrogel. Lastly, we took advantage of the stable adhesion to tissues *in vivo* and designed internal bandages for either anti-tumor drug delivery or type 1 diabetes cell replacement therapy. We showed the biodegradable hydrogel

bandage encapsulating human serum albumin conjugated cisplatin enabled drug delivery directly to the tumor site, improved the pharmacokinetics and lead to a higher treatment efficacy with less side effects in an orthotopic liver cancer model. On the other hand, the none-degradable hydrogel bandage provided a unique solution to the delivery of insulin-producing cells, circumventing the problem of settling and clumping faced by conventional hydrogel microparticles or the issue of folding and crumpling encountered by hydrogel sheets. While more work is required to translate our adhesive hydrogels into clinical applications, this study provides a proof of concept for their potential use in developing internal bandages for drug and cell delivery.

Supplementary Material

Refer to Web version on PubMed Central for supplementary material.

Acknowledgements

This work was partially supported by the National Institutes of Health (NIH, 1R01DK105967-01A1), the Novo Nordisk Company, the Juvenile Diabetes Research Foundation (JDRF, 2-SRA-2018-472-S-B) and the Hartwell Foundation.

References

[1]. a) Conde J, Oliva N, Atilano M, Song HS, Artzi N, Nat. Mater 2016, 15, 353; [PubMed: 26641016] b) Sepantafar M, Maheronnaghsh R, Mohammadi H, Radmanesh F, Hasani-Sadrabadi MM, Ebrahimi M, Baharvand H, Trends Biotechnol. 2017, 35, 1074; [PubMed: 28734545] c) Li J, Mooney DJ, Nat. Rev. Mater 2016, 1, 16071. [PubMed: 29657852]

[2]. a) Weaver JD, Headen DM, Aquart J, Johnson CT, Shea LD, Shirwan H, García AJ, Sci. Adv 2017, 3, e1700184; [PubMed: 28630926] b) Bochenek MA, Veiseh O, Vegas AJ, McGarrigle JJ, Qi M, Marchese E, Omami M, Doloff JC, Mendoza-Elias J, Nourmohammadzadeh M, Nat. Biomed. Eng 2018, 2, 810; [PubMed: 30873298] c) Zhang Y, An D, Pardo Y, Chiu A, Song W, Liu Q, Zhou F, McDonough SP, Ma M, Acta Biomater. 2017, 53, 100; [PubMed: 28216297] d) Fuchs S, Shariati K, Ma M, Adv. Healthc. Mater 2020, 9, 1901396.

[3]. a) Roshanbinfar K, Vogt L, Greber B, Diecke S, Boccaccini AR, Scheibel T, Engel FB, Adv. Funct. Mater 2018, 28, 1803951;b) McLaughlin S, McNeill B, Podrebarac J, Hosoyama K, Sedlakova V, Cron G, Smyth D, Seymour R, Goel K, Liang W, Nat. Commun 2019, 10, 1. [PubMed: 30602773]

[4]. Yang J, Bai R, Chen B, Suo Z, Adv. Funct. Mater. 2020, 30, 1901693.

[5]. Li J, Celiz A, Yang J, Yang Q, Wamala I, Whyte W, Seo B, Vasilyev N, Vlassak J, Suo Z, Science 2017, 357, 378. [PubMed: 28751604]

[6]. Yuk H, Varela CE, Nabzdyk CS, Mao X, Padera RF, Roche ET, Zhao X, Nature 2019, 575, 169. [PubMed: 31666696]

[7]. a) Lee H, Dellatore SM, Miller WM, Messersmith PB, Science 2007, 318, 426; [PubMed: 17947576] b) Cholewinski A, Yang FK, Zhao BJMH, Mater. Horiz 2019, 6, 285.

[8]. Liang S, Zhang Y, Wang H, Xu Z, Chen J, Bao R, Tan B, Cui Y, Fan G, Wang W, Adv. Mater 2018, 30, 1704235.

[9]. Gan D, Xing W, Jiang L, Fang J, Zhao C, Ren F, Fang L, Wang K, Lu X, Nat. Commun 2019, 10, 1487. [PubMed: 30940814]

[10]. Maier GP, Rapp MV, Waite JH, Israelachvili JN, Butler A, Science 2015, 349, 628. [PubMed: 26250681]

[11]. Zhang T, Yuk H, Lin S, Parada GA, Zhao X, Acta Mech. Sin 2017, 33, 543.

[12]. a) Wei Y, J. Mech. Phys. Solids 2014, 70, 227;b) Vernerey F. J. J. J. o. t. M., Solids P. o., J. Mech. Phys. Solids 2018, 115, 230; [PubMed: 31680703] c) Yang T, Yang X, Huang R, Liechti KM, J Journal of the Mechanics and Physics of Solids 2019, 131, 1.

[13]. Möller JJ, Bitzek E, Janisch R, ul Hassan H, Hartmaier A, J. Mater. Res 2018, 33, 3750.

[14]. Giano MC, Ibrahim Z, Medina SH, Sarhane KA, Christensen JM, Yamada Y, Brandacher G, Schneider JP, Nat. Commun 2014, 5, 4095. [PubMed: 24958189]

[15]. a) Siegel RL, Miller KD, Jemal A, CA Cancer J. Clin 2019, 69, 7; [PubMed: 30620402] b) Huo D, Zhu J, Chen G, Chen Q, Zhang C, Luo X, Jiang W, Jiang X, Gu Z, Hu Y, Nat. Commun 2019, 10, 1. [PubMed: 30602773]

[16]. Liu P-H, Hsu C-Y, Hsia C-Y, Lee Y-H, Huang Y-H, Chiou Y-Y, Lin H-C, Huo T-I, Ann. Surg 2016, 263, 538. [PubMed: 25775062]

[17]. a) Llovet JM, Zucman-Rossi J, Pikarsky E, Sangro B, Schwartz M, Sherman M, Gores G, Nat. Rev. Dis. Primers 2016, 2, 16018; [PubMed: 27158749] b) Spolverato G, Vitale A, Bagante F, Connolly R, Pawlik TM, Ann. Surg 2017, 265, 792. [PubMed: 28266967]

[18]. a) He C, Tang Z, Tian H, Chen X, Adv. Drug Deliv. Rev 2016, 98, 64; [PubMed: 26546464] b) Liu J, Chang B, Li Q, Xu L, Liu X, Wang G, Wang Z, Wang L, Adv. Sci 2019, 6, 1801987.

[19]. Shi H, Cheng Q, Yuan S, Ding X, Liu Y, Chem. Eur. J 2015, 21, 16547. [PubMed: 26405808]

[20]. Kratz F, J. Control. Release 2008, 132, 171. [PubMed: 18582981]

[21]. a) Brown SA, Kovatchev BP, Raghinaru D, Lum JW, Buckingham BA, Kudva YC, Laffel LM, Levy CJ, Pinsker JE, Wadwa RP, N. Engl. J. Med 2019, 381, 1707; [PubMed: 31618560] b) Yu J, Zhang Y, Ye Y, DiSanto R, Sun W, Ranson D, Ligler FS, Buse JB, Gu Z, Proc. Natl. Acad. Sci. U.S.A 2015, 112, 8260; [PubMed: 26100900] c) Shapiro AJ, Pokrywczynska M, Ricordi C, Nat. Rev. Endocrinol 2017, 13, 268. [PubMed: 27834384]

[22]. Ernst AU, Bowers DT, Wang L-H, Shariati K, Plesser MD, Brown NK, Mehrabyan T, Ma M, Adv. Drug Deliv. Rev 2019, 139, 116. [PubMed: 30716349]

[23]. a) Bochenek MA, Veiseh O, Vegas AJ, McGarrigle JJ, Qi M, Marchese E, Omami M, Doloff JC, Mendoza-Elias J, Nourmohammadzadeh M, Nat. Biomed. Eng 2018, 2, 810; [PubMed: 30873298] b) Liu Q, Chiu A, Wang L-H, An D, Zhong M, Smink AM, de Haan BJ, de Vos P, Keane K, Vegge A, Nat. Commun 2019, 10, 1; [PubMed: 30602773] c) An D, Chiu A, Flanders JA, Song W, Shou D, Lu Y-C, Grunnet LG, Winkel L, Ingvorsen C, Christophersen NS, Proc. Natl. Acad. Sci. U.S.A 2018, 115, E263. [PubMed: 29279393]

[24]. Cui C, Wu T, Gao F, Fan C, Xu Z, Wang H, Liu B, Liu W, Adv. Funct. Mater 2018, 28, 1804925.

[25]. Liu X, Zhang Q, Gao G, Adv. Funct. Mater 2017, 27, 1703132.

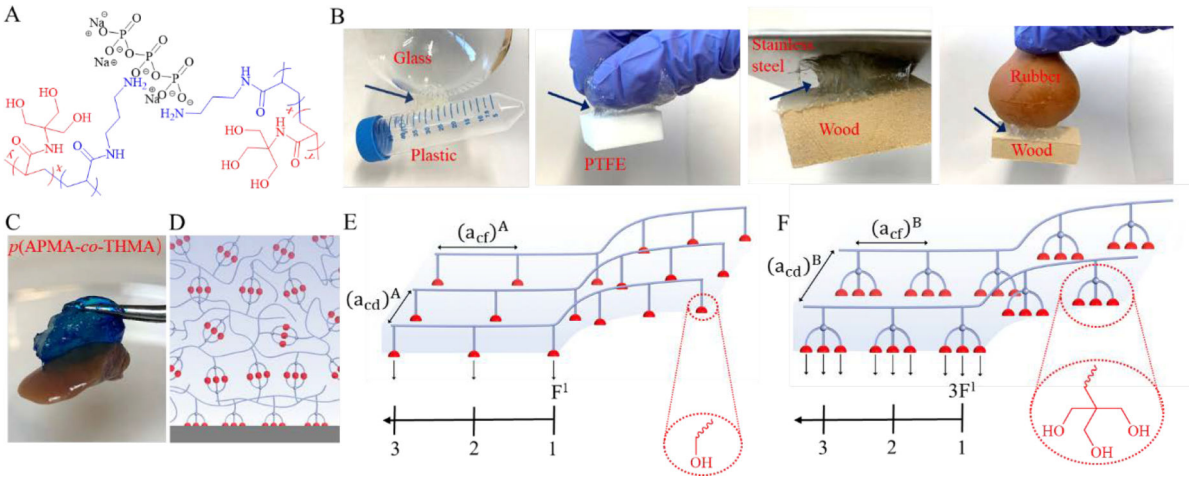

Figure 1.

A) A schematic of *p*(APMA-*co*-THMA) crosslinked with STTP to form adhesive hydrogel. B) Photos of the THBC adhesive hydrogel sticking to glass flask, plastic tube, PTFE sheet, stainless steel sheet, wood block and rubber. C) Adhesion of the THBC hydrogel (mixed with a blue food dye) to mice liver. D) Dynamic hydrogen bond clusters dissipating energy at both interface and the bulk. E) Homogeneously distributed hydrogen bonding with equal bond density as the THBC hydrogel. F) The load sharing of the THBCs making the crack at the interface harder to propagate (See detailed analysis in Supplemental Information.)

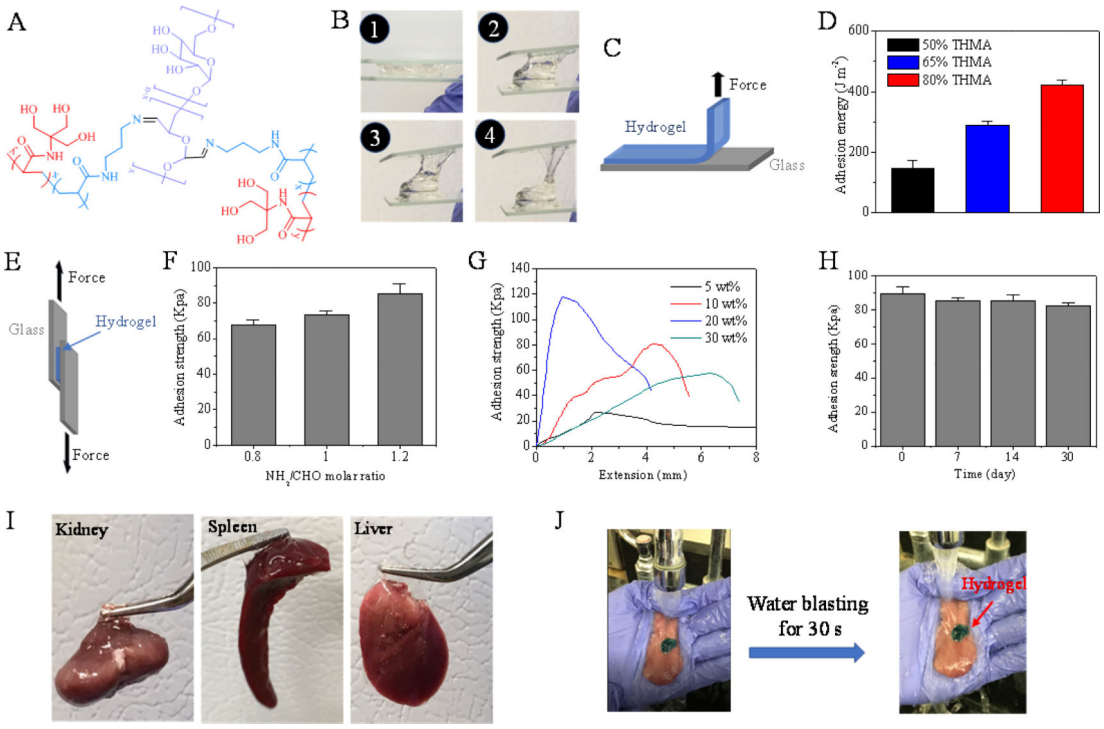

Figure 2.

A) A schematic of *p*(APMA-*co*-THMA) crosslinked with Dex-CHO to form biodegradable adhesive hydrogel. B) The adhesive property of the hydrogel between two glass slides. C) A schematic of the peeling test. D) Average adhesive energy of hydrogels with different THMA contents to glass slide as measured by the peeling test. E) A schematic of the lap shear test. F) Adhesion strength of 80% THMA hydrogels with different NH_2/CHO molar ratios and G) with different solid contents. H) Change of adhesion strength of the hydrogel in saline over a month. I) Adhesion to various tissues including kidney, spleen and liver. J) Adhesion of the hydrogel (mixed with a blue food dye) to rat liver under running water for 30s.

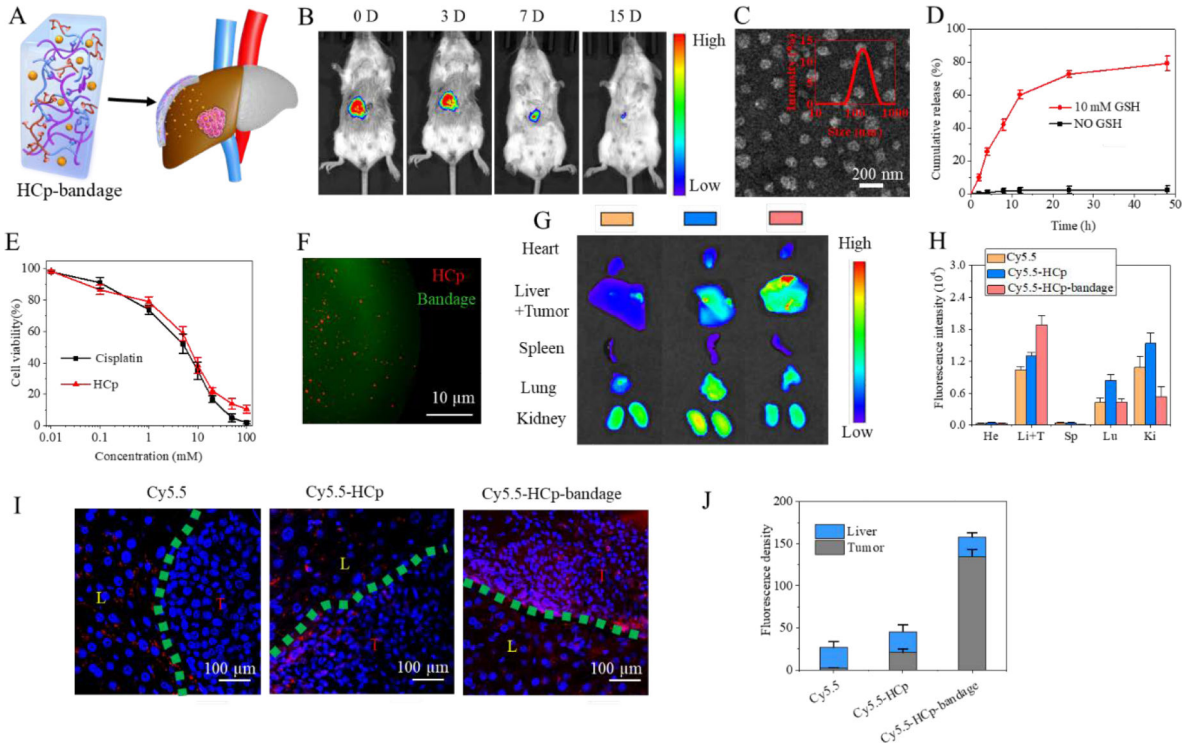

Figure 3.

A) A schematic of HCp-bandage applied on the surface of orthotopic luciferase-expressing HepG2 (Luc-HepG2) liver tumor bearing liver. B) *In vivo* biodegradation behavior of Cy5.5 labelled bandage after 15 days, n=3. C) TEM image and size distribution of HCp nanoparticles. D) *In vitro* drug release of HCp nanoparticles with and without 10 mM GSH. E) Cell cytotoxicity of HCp nanoparticles. F) Representative fluorescent images of a HCp-loaded adhesive hydrogel bandage, in which the hydrogel was labelled with FITC and HCp nanoparticles were labelled with Cy5.5. G) Biodistribution and H) quantitative analysis of Cy5.5, Cy5.5-HCp and Cy5.5-HCp-bandage in tissues after 3 Days, n=3. I) Fluorescent imaging and J) quantitative analysis of fluorescence distribution in liver and tumor after 3 Day, n=3.

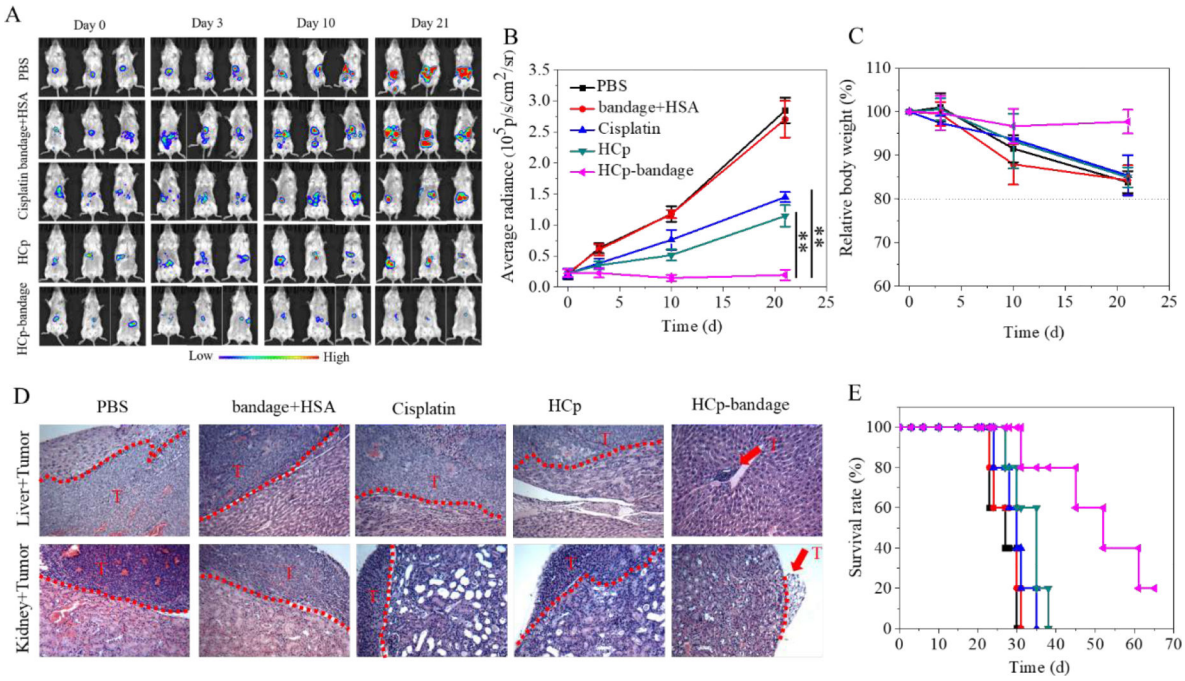

Figure 4.

A) Tumor volume changes evaluated by bioluminescence imaging in mice treated with HCp-bandage, HCp, Cisplatin, blank bandage with HSA, and PBS. (n=6; other 3 mice from each group are shown in SI) B) Quantitative analysis of average bioluminescence levels of the mice in different treatment groups. C) Body weight changes of mice over 20 days. D) H&E staining of liver and kidney sections excised from tumor-bearing mice following treatment with HCp-bandage, HCp, Cisplatin, blank bandage with HSA, and PBS for 21 days. E) Survival rates of mice after 60 days.

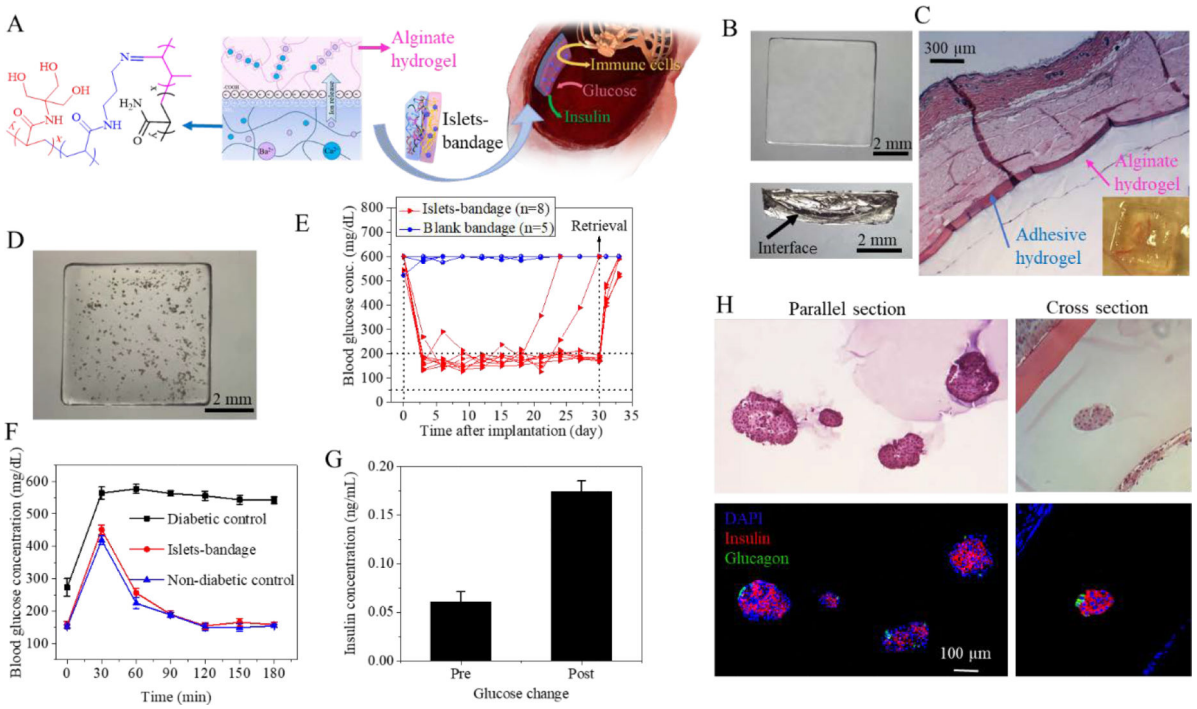

Figure 5.

A) A schematic of the islet bandage: an adhesive hydrogel layer and an islet-encapsulating layer. B) Top view and side view of a blank bilayer hydrogel bandage. C) Representative H&E image of blank hydrogel bandage adhering to the peritoneal cavity wall after 10 days (inset: a macroscopic photo). D) Top view of rat islets loaded adhesive bandage. E) BG concentrations of mice during 30 days of transplantation. F) IPGTT on day 20. G) *Ex vivo* GSIS test of the retrieved rat islets. H) H&E and immunostaining images of rat islets in retrieved samples.